



Power train degradation modelling for multi-objective active power control of wind farms

Farid K. Moghadam¹ · Valentin Chabaud² · Zhen Gao¹ · Spyridon Chapaloglou²

Received: 2 November 2022 / Accepted: 11 January 2023 / Published online: 20 March 2023
© The Author(s) 2023

Abstract

With the coming installation of hundreds of GW of offshore wind power, penetration of the inherent power fluctuations into the electricity grid will become significant. Therefore, the use of wind farms as power reserve providers to support the regulation of the grid's voltage and frequency through delivering a desired power is expected to increase. As a result, wind turbines will not be necessarily delivering the maximum available power anymore – known as curtailed or derated operation – and will have to be able to deal with time-variant power demand. For this purpose, power setpoints from the grid are dispatched at the farm-level and then tracked at the turbine-level under the constraint of available power in the wind (known as active power control). The idea of this work is taking advantage of the additional degree of freedom lying in the power dispatch between turbines when operating in curtailed conditions. As failure of power train system components is frequent, costly and predictable, we seek to introduce power train degradation into the farm control objectives. To this end, a data-driven model of drivetrain fatigue damage as function of wind conditions and derating factor adapted to the farm active power control objective function is developed based on the pre-analysis of single-turbine simulations and degradation calculations, where the increased turbulence intensity due to wind farm wake effect is also considered. The proposed analytical power train degradation model is computationally efficient, can reflect the fatigue damage of individual gears and bearings in the overall power train life function and in contrast with high-fidelity models can be easily adjusted for different drivetrain configurations. A case study on the TotalControl reference wind power plant is demonstrated.

✉ Farid K. Moghadam
farid.k.moghadam@ntnu.no

Valentin Chabaud
valentin.chabaud@sintef.no

Zhen Gao
zhen.gao@ntnu.no

Spyridon Chapaloglou
spyridon.chapaloglou@sintef.no

¹ Department of Marine Technology, Norwegian University of Science and Technology, Jonsvannsveien 82, 7050 Trondheim, Norway

² Energy Systems Department, SINTEF Energy Research, Sem Sæleands veg 11, 7034 Trondheim, Norway

Modellierung der Degradation des Antriebsstrangs für aktive multiobjektive Leistungsregelung von Windparks

Zusammenfassung

Mit der bevorstehenden Installation von Hunderten von Gigawatt Offshore-Windenergie werden die inhärenten Leistungsschwankungen im Stromnetz erheblich zunehmen. Daher wird erwartet, dass Windparks zunehmend als Leistungsreserve eingesetzt werden, um die Regulierung der Netzspannung und -frequenz durch die Lieferung einer gewünschten Leistung zu unterstützen. Infolgedessen werden Windturbinen nicht mehr unbedingt die maximal verfügbare Leistung liefern können – bekannt als “curtailed” oder “derated” Betrieb – und müssen in der Lage sein, mit zeitlich schwankendem Leistungsbedarf umzugehen. Zu diesem Zweck werden Leistungssollwerte aus dem Netz auf der Parkebene vorgegeben und dann auf der Turbinenebene unter der Bedingung der verfügbaren Windleistung nachgeführt (sogenannte aktive Leistungsregelung oder “active power control”). Die Idee dieser Arbeit ist es, den zusätzlichen Freiheitsgrad zu nutzen, der in der Leistungsverteilung zwischen den Turbinen liegt, wenn diese unter eingeschränkten Bedingungen betrieben werden. Da Ausfälle von Komponenten des Antriebsstrangs häufig, kostspielig und vorhersehbar sind, versuchen wir, die Verschlechterung des Antriebsstrangs in die Steuerungsziele des Parks einzubeziehen. Zu diesem Zweck wird ein datengesteuertes Modell der Ermüdungsschäden des Antriebsstrangs als Funktion der Windbedingungen und des Abminderungsfaktors entwickelt, das an die Zielfunktion der Leistungsregelung des Parks angepasst ist und auf der Voranalyse von Simulationen und Degradationsberechnungen für eine einzelne Turbine basiert, wobei auch die erhöhte Turbulenzintensität aufgrund des Windpark-Wake-Effekts berücksichtigt wird. Das vorgeschlagene analytische Degradationsmodell für den Antriebsstrang ist rechnerisch effizient, kann die Ermüdungsschäden einzelner Zahnräder und Lager in der Gesamtlebensdauerfunktion des Antriebsstrangs widerspiegeln und lässt sich im Gegensatz zu High-Fidelity-Modellen leicht an unterschiedliche Antriebsstrangkonfigurationen anpassen. Eine Fallstudie an der TotalControl-Referenz-Windkraftanlage wird demonstriert.

1 Introduction

The power train system consisting of back-to-back (BTB) frequency converter, generator, gearbox, shafts, main bearings and rotor is in average responsible for more than 50% of the wind turbine total failures and downtime [34]. Therefore mitigating the degradation of this system through improving operation by employing holistic optimal control can contribute significantly to the leveled cost of energy (LCOE).

For a given power train system, the literature proves that it is possible to manipulate the power train system loads and therefore life through modifying the control. Even though the literature is mainly focused on the turbine level controllers, namely the torque, pitch [8] and generator control [27] to mitigate the power train load oscillations and improving lifetime, there is also potential at the farm level through a smarter power dispatch. A major advantage there is feasibility: power dispatch is at the hands of farm operators, while turbine controllers are proprietary to turbine manufacturers and hard to change.

Wind farm active power control (APC) focuses on following a reference power commanded from the grid. This may be realized in open- or closed-loop, with or without defining an optimization problem [23]. A detailed review on different available wind farm APC design techniques is presented by [35]. Depending on the local wind conditions (turbulent fluctuations), multiple combinations (dispatches) of turbine-level power setpoints may yield the desired farm-

level power reference. This degree-of-freedom may be exploited to mitigate fatigue damage of different components of turbine such as tower, blades and power train.

Different methods for modelling turbine components fatigue damage, and eventually designing the multi-objective farm controller have been proposed in the literature. Baros and Annaswamy in [2] define a damage cost function in the farm power tracking design aimed at minimizing the damage loads. The limitation of the optimization approach in general is that it is not possible to describe the fatigue loads of all the components as closed form expressions of turbine power. Another strategy is to tune the farm power tracking feedback control by defining adaptive gains based on penalizing the turbines with higher mean values of damage equivalent load in the power tracking decision making time steps as reported by [25, 37]. All the aforesaid works are focused on structural damage by using either load directly or damage equivalent load. The data-based control design strategy for tuning the controller by using the estimated fatigue for turbine damage mitigation is originally proposed by [21].

The main motivation for this work is to include power train fatigue damage into the APC algorithm in a practical decoupled manner by using a database. It is not meant to be used directly for the design of power train under actual wind conditions, relaxing accuracy requirements. Power train system combines a wide range of electrical, electronics and mechanical components. In this research, the focus is on bearings and gear transmission called drivetrain which

has the highest contribution in turbine downtime and a considerable contribution in the overall failure rate per turbine per year [34], and a high coupling between the dynamics of these mechanical rotating components with the aerodynamic-induced loads [3]. Main bearings, gearbox high-speed shaft (HSS) bearings and the gears reported as the components with the highest contribution in the drivetrain failures [9, 11, 38], which in addition to generator bearings are considered in the power train system damage analysis in this paper. Bearings are the most frequently failed component in the electric machines [40]. Even though the generator bearings of wind turbines with a rated power higher than 2MW are in average responsible for more than 50% of generator failures [36], which must handle the wind generator’s highly variant electromagnetic forces, have not been attracting research attentions given the more simple design and possibility to overdesign these bearings [39].

The main contributions of this paper are

- Proposing a database approach for accommodating power train system damage in wind farm active power control,
- Proposing computationally efficient physical models driven by power train input loads time series data for estimating load, stress and analyzing fatigue damage due to different failure modes for individual gears and bearings of power train,
- Demonstrating multi-objective APC based on the proposed approach and average improvement in turbine overall life,
- Proposing different damage indices as the indication of overall damage in the power train of wind turbines,
- Integrating the generator bearings into the drivetrain damage analysis.

The remainder of the paper is organized as follows. Sect. 2 describes the proposed database approach for integrating power train system fatigue damage into the farm active power control design. The power train degradation

model and the procedure for the creation of database are also discussed in this section. The results related to the implementation of the proposed power train system degradation analysis, the fatigue damage database as a function of external conditions, and the demonstration of the possibility of the farm-wide utilization of damage database for flattening damage between turbines for improving the farm availability are discussed in Sect. 3. Finally the paper is concluded in Sect. 4.

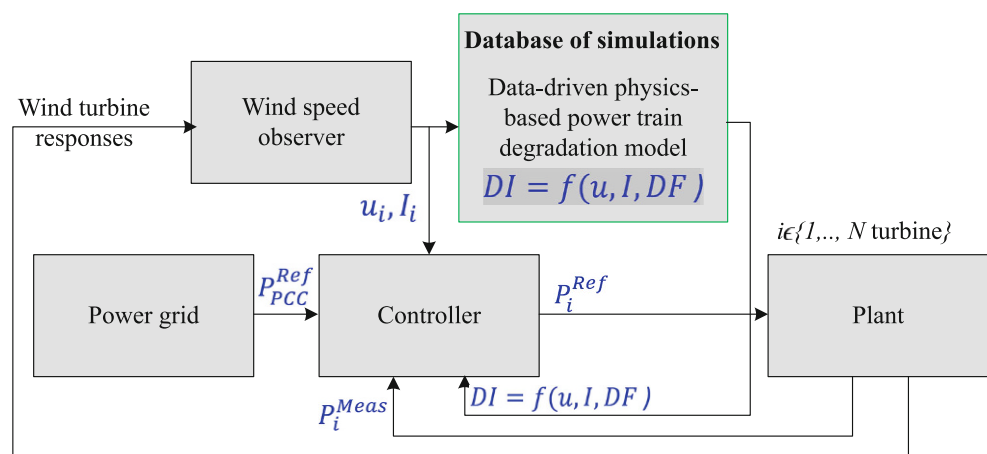
2 Methodology

To use damage in real-time control decisions, the damage indicator can be calculated online (by using online load observers) or extracted from a pre-calculated database. High uncertainties in estimation of power train system loads in practice and the required computational resources are motivations for using an offline rather than online approach in this work. Damage in power train system components is estimated by using physics-based simulations supported by analytical models describing the behavior of system and components. The database approach is then mapping the turbine’s environmental and operational conditions to power train system damage. It is constructed by using the simplest form of surrogate modelling: a look-up table with linear interpolation on an evenly discretized parameter space. The database can then be used in farm simulations and real-world farm controllers, making use of damage indicators for each turbine exposed to different external conditions, in order to improve the overall fatigue life and maintenance planning of the farm.

2.1 Framework

The block-diagram illustrating the utilization of the proposed database approach for accommodating the power train system damage in farm APC is illustrated in Fig. 1.

Fig. 1 Database approach for accommodating power train damage in farm control design



The power train degradation database generated from extensive turbine-level simulations in all possible combinations of power demand and wind speed conditions is used for tuning the farm power tracking controller. u and I are the average wind speed and turbulence intensity. DF stands for derating factor which is defined as

$$DF = \frac{GenPwr}{P^{avail}} : P^{avail} = \min \left\{ \frac{1}{2} C_p^{max} \rho A u(t)^3, P^{rated} \right\}, \quad (1)$$

where P^{avail} is the turbine available power which is saturated when it goes to higher than rated power P^{rated} . $GenPwr$ is the mean value of turbine generated power. $u(t)$ is instantaneous wind speed, C_p^{max} is the maximum electrical power coefficient, A is the area covered by the rotor (m^2) and ρ is the air density (kg/m^3).

Use at farm level is as follows: wind speeds accounting for wake velocity deficit and derating factors for each turbine are run through a 10-minutes moving average filter. Turbulence intensity may be observed from the turbine’s response or derived from wind speed (it requires a bit more

care in order to account for wake effects, see Sect. 2.4). Linear interpolation is used to read in the 10-min accumulated damage from the database.

Details on the creation of database, power train fatigue damage modelling and multi-objective active power control of wind farm by using power train degradation database are presented in the following sections.

2.2 Turbine-level database

The procedure for the creation of power train fatigue damage database is summarized by the block diagram in Fig. 2. As it can be seen, to generate the database, a fully-coupled wind turbine simulation model in OpenFAST is used including a simplified power train model and loading a custom version of the DTU wind energy controller featuring active power derating functionality [10]. This model is exposed to input turbulent wind field model generated by TurbSim. This model provides the power train input loads as listed in Fig. 2, which then feed quasi-static models describing the power train components load as the main input for damage analysis.

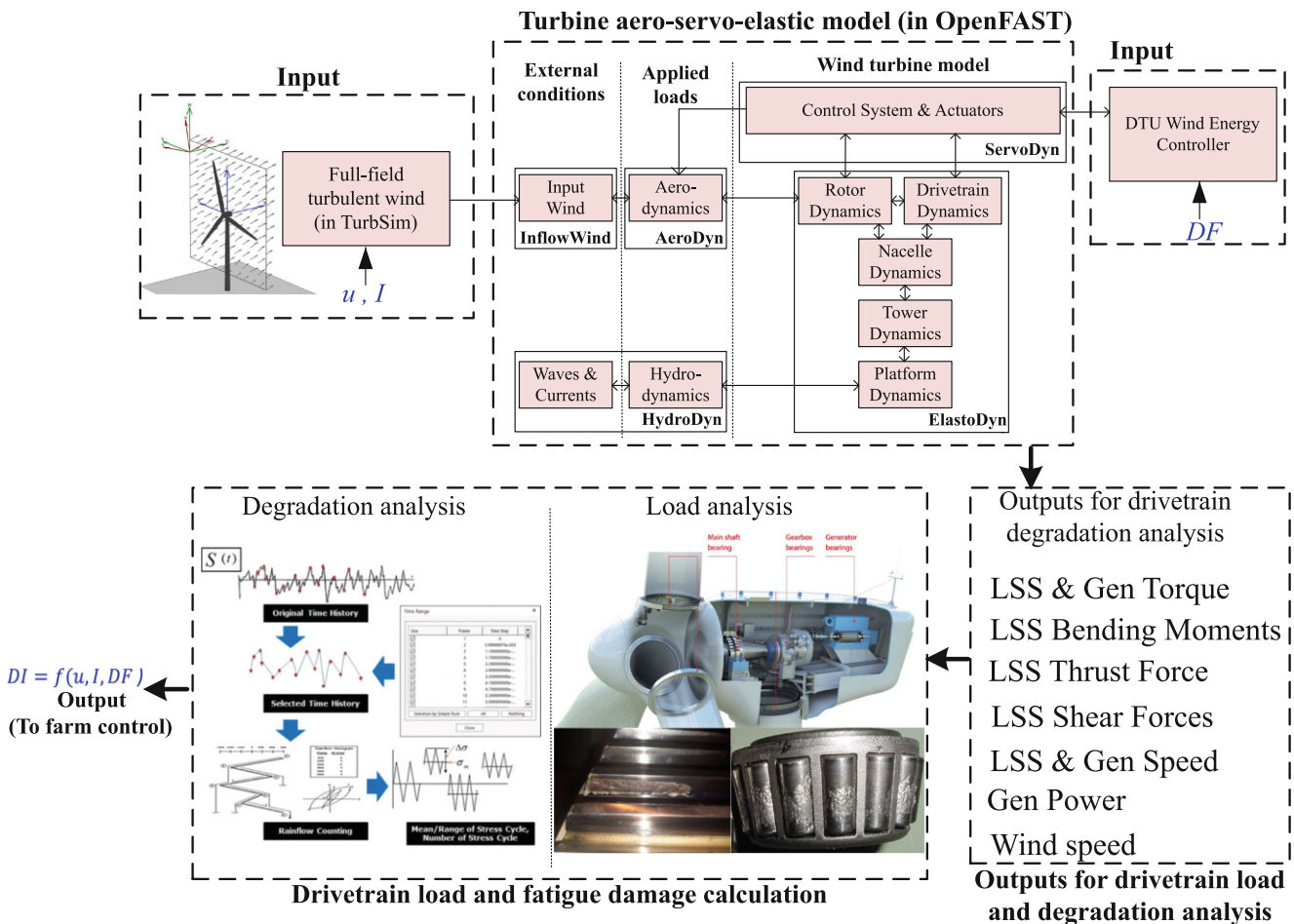


Fig. 2 Power train damage vs. wind speed and power command database generation by single-turbine simulation

The damage indicator can be developed on damage equivalent load (DEL) for structural damage analysis [29], but for the power train system components, namely bearings and gears this method is not utilized. The standard approach for the bearing degradation analysis is based on estimation of dynamic equivalent load and using the bearing life equation, while for gears damage is calculated based on the maximum damage between the damage due to pitting and the one due to root bending stress [28, 38]. For the gears and bearings the damage is calculated by applying Palmgren-Miners rule to the stress and load time series, respectively. The utilized damage estimation theories are explained in more detail in the associated sections.

2.2.1 System description

The turbine model developed in NREL's OpenFAST is a detailed coupled aero-hydro-servo elastic dynamic model containing the structural and power train dynamics used to calculate wind turbine loads as the main input for the power train fatigue damage analysis. The latter is able to capture the influence of three dimensional flow on the blade, unsteady aerodynamic effects, structural dynamics and the coupling of vibration modes of different subsystems, aeroelastic effects and the behaviour of the control system of the wind turbine. More details about OpenFAST global load and response analysis can be found in [31]. The three dimensional turbulent wind field is modelled by NREL's TurbSim, where the turbulence model is based on Kaimal spectrum and exponential coherence model. The wind flow parameters and boundary conditions are obtained from IEC 61400-1 [13] and IEC 61400-3 [14] for bottom fixed turbines in offshore fields, where the mean wind speed is changing from cut-in to cut-out speeds to cover different possible wind speeds, and the reference value of the turbulence intensity corresponding to the 70% quantile at 15 m/s turbulence intensity is changed in a wide range to account for different turbulence categories to make the results extendable to different sites and wake conditions¹ (see Sect. 2.1). Wave loads are currently absent for simplicity, but may be included in further work.

The power train configuration assumed for fatigue damage analysis is double main bearing with four point suspension [12]. The power train selection of gears, main bearings and gearbox bearings which influences the distribution of loads in the drivetrain components is based on the work [38]. The methodology and the analytical models for

load calculation can be extended to various configurations with minor modifications.

2.2.2 Turbine control

The turbine controller is responsible for tracking the power setpoints given by the farm APC, provided that there is enough available power in the incoming wind. Wind turbine operation may be divided into two regimes: partial-load (power maximization) and full-load (power tracking). As the rotor speed approaches a reference value (in normal operation, the rated rotor speed), the turbine enters full-load operation. The controller then tracks the reference rotor speed by pitching the blades while the power is held constant (in normal operation, to the rated power) by adjusting the generator torque. In derated operation, the transition between the two regimes is not dictated by rated power and rated rotor speed, but rather by the desired power and a custom reference rotor speed. The choice of the latter corresponds to different derating strategies. Various methods may be used to this end [5, 21, 35]. The power-speed curve method used in this research sets the choice of rotational speed as variable along the torque-speed curve in normal operation and always ensures operating around the combinations of power and rotor speed that are seen in normal operation. It is hence considered as closest to how industrial wind turbine controllers operate and is selected in this study for this reason. Assuming the updated derated power demand $P_{derated} \in P_{derated} \in R \mid P_{min} \leq P_{derated} < P_{rated}$, by using torque-speed relationship in normal partial-load operation, the updated derated rotor speed $\omega_{derated}$ is calculated by

$$\omega_{derated} := \min \left\{ \sqrt[3]{\frac{P_{derated}}{\frac{1}{2}\rho A C_P^{max}} \frac{\lambda_{opt}}{r}}, \omega_{rated} \right\} \quad (2)$$

This method acts as above-rated operation with variable rated rotor speed. The torque controller matches the desired power $P_{derated}$, and the pitch controller tracks the rotor speed $\omega_{derated}$ that always corresponds to a torque-speed operating point found in normal operation (where the transition and cut-in regions have been simplified).

2.3 Power train system degradation modelling

There are numerical [22, 38] and analytical methods [9, 28] that can be used for drivetrain gear and bearing load analysis. Here it is the analytical methods that are used. The methodology is generic and can be used on any wind turbine power train design. In this study we focus on the DTU 10MW reference wind turbine.

As discussed earlier, the drivetrain loads are calculated from fully-coupled turbine- power train dynamic model.

¹ Note that the Kaimal spectrum takes also a time constant $\frac{\Delta}{u}$ (with Δ a constant characteristic length) as input parameter in addition to turbulence intensity. This will not be properly accounted for when the database is looked up in wake conditions with lower wind speed u , but the induced error is deemed negligible.

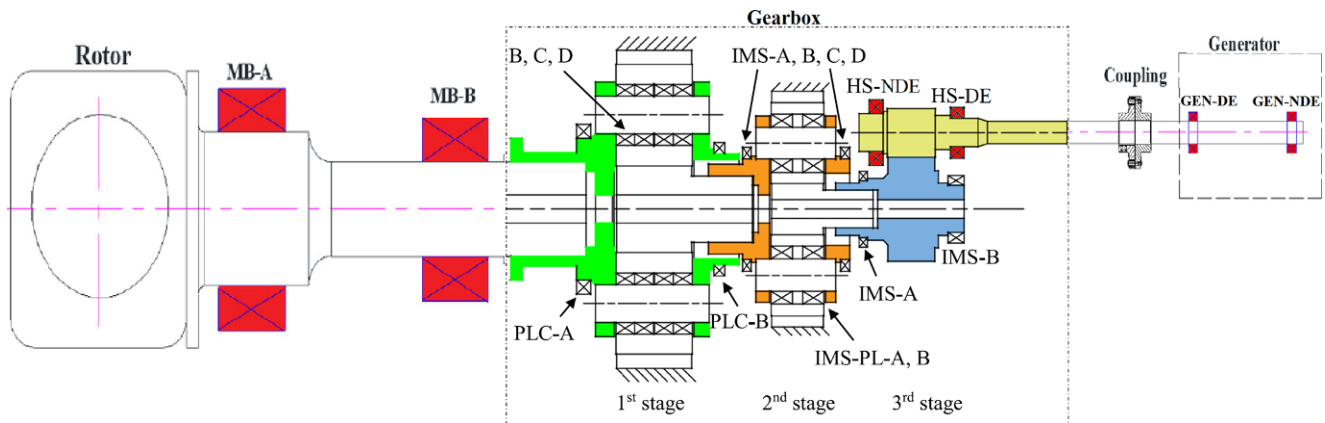


Fig. 3 Drivetrain system layout (Adopted from [38])

However, the estimation of each gear and bearing load in the power train layout is based on quasi-static assumption, meaning that at a given instant in time the problem is assumed to be static. In other words, when translating the drivetrain input loads to the individual gears and bearings loads, the internal inertial, stiffness and damping forces of the individual components are neglected.

2.3.1 Power train system load calculation

There are numerical [22, 38] and analytical methods [21, 28, 32, 33] that can be used for drivetrain gear and bearing load analysis. Authors in [33] proposed a portable modelling approach to calculate the drivetrain loads, which separates the parameter and analysis spaces, and show that with a restricted parameter set it is still possible to calculate accurately the drivetrain loads as the input for drivetrain reliability analysis. Here it is the analytical methods that are used. The power train configuration and the choice of gears and bearings has a significant influence on the components load and damage. The drivetrain configuration and the selection of gears, gearbox bearings and main bearings are based on the design proposed by [38]. Based on this design, the gearbox is three stages based on two planetary one parallel gear stages. The main bearings are based on tapered roller bearings (TRB). The gearbox HSS non-drive end (NDE) bearing is cylindrical roller bearing (CRB), and the drive end (DE) bearing is TRB. The generator bearings are both deep groove ball bearings which are exposed to high cycle fatigue. The skf 360141 bearing is selected as generator bearings. The bearing selection was done based on a compromise between shaft diameter and operating speed and basic dynamic load rating. and available solutions in industry. A customized design which could handle a higher basic dynamic load rating could demonstrate a better performance in life. The basic dynamic load rating was calculated based on average load based on load time series analysis, the de-

sired lifespan and operating speed. It is assumed electrical erosion due to stay currents is avoided by taking sufficient measures during installation. The selection of coupling influences the forces in generator bearings. For this purpose, KTR Revolex KX-D 330 standard coupling is selected because of its high torque capacity, low torsional flexibility, backlash free and fail safe feature and the possibility to add disk brake to it. The coupling torque is selected based on the rated and peak torques of the driving side and applying sufficient safety factors. The drivetrain configuration is shown in Fig. 3. The bearings considered in the fatigue damage analysis are highlighted in red.

Gears load calculation theory: The load is calculated independently for each of the gears in the drivetrain gearbox, the 1st gear stage consists of a sun, five planets and a ring, the 2nd stage of a sun, three planets and a ring and the 3rd stage of a wheel and a pinion. The load in the planets are assumed to be identical which leads to eight different gears for life calculation studies in this work. Gear tooth contact and root bending are two common fatigue failure mechanisms of the gears in wind turbine gearboxes, which are considered in this research. The other gear failure mechanisms including micropitting, scuffing and wear are not in the scope of this paper. In this work, the procedure to

Table 1 Drivetrain torque calculation from input rotor torque

Gear	EQ
Planet-Stage1	$T_{planet-s1} = \frac{1}{(1 - \frac{Z_{ring1}}{Z_{planet1}})} T_R$
Sun-Stage1	$T_{sun-s1} = -\frac{1}{\alpha_1} T_R, \alpha_1 = 1 + \frac{Z_{ring1}}{Z_{sun1}}$
Ring-Stage1	$T_{ring-s1} = -\frac{Z_{ring1}}{Z_{sun1} + Z_{ring1}} T_R$
Planet-Stage2	$T_{planet-s2} = \frac{1}{\alpha_1} \frac{1}{(1 - \frac{Z_{ring2}}{Z_{planet2}})} T_R$
Sun-Stage2	$T_{sun-s2} = -\frac{1}{\alpha_1 \alpha_2} T_R, \alpha_2 = 1 + \frac{Z_{ring2}}{Z_{sun2}}$
Ring-Stage2	$T_{ring-s2} = -\frac{1}{\alpha_1} \frac{Z_{ring2}}{Z_{sun2} + Z_{ring2}} T_R$
Wheel-Stage3	$T_{wheel-s3} = \frac{1}{\alpha_1 \alpha_2} T_R$
Pinion-Stage3	$T_{pinion-s3} = \frac{1}{\alpha_1 \alpha_2 \alpha_3} T_R, \alpha_3 = \frac{Z_{wheel}}{Z_{pinion}}$

calculate contact and root bending stress are according to ISO standards 6336-2 and 6336-3 [17, 18], respectively. In this procedure, the gear root bending and pitting stresses are functions of the gear input torque and geometry. The gear pitting stress at pitch point and root bending stress of the gear i ($\forall i \in \{1, \dots, 8\}$) can be calculated by [17, 18]

Pitting: $\sigma_{Hi} = Z_{Hi} Z_{Ei} Z_{\epsilon i} Z_{\beta i}$
 $\times \sqrt{K_{Ai} K_{\gamma i} K_{vi} K_{H\beta i} K_{H\alpha i}} \sqrt{\frac{F_{ti}}{b_i d_{i1}} \frac{u_i + 1}{u_i}}$, (3a)

Root bending: $\sigma_{Fi} = Y_{Fi} Y_{Si} Y_{\beta i} Y_{Bi} Y_{DTi}$
 $\times K_{Ai} K_{\gamma i} K_{vi} K_{F\beta i} K_{F\alpha i} \frac{F_{ti}}{b_i m_{ni}}$, (3b)

where F_t is the transverse tangential load which can be calculated based on ISO 6336-1:2019 [16] as a function of i th gear input torque T_i by $F_{ti} = \frac{2000T_i}{d_{i1}}$. The calculation of T_i for all the gears from the rotor input torque is based on the equations summarized in Table 1.

The representations in Eq. can be simplified as [28]

$$\sigma_{Hi} = \sigma_{HNi} \sqrt{\left| \frac{T_i}{T_{Ni}} \right|}, \tag{4a}$$

$$\sigma_{Fi} = \sigma_{FNi} \left| \frac{T_i}{T_{Ni}} \right|, \tag{4b}$$

where σ_{Hi} and σ_{Fi} are defined in terms of nominal contact and bending stress σ_{HNi} and σ_{FNi} , and nominal torque T_{Ni} , as defined by

$$\sigma_{HNi} = Z_{Hi} Z_{Ei} Z_{\epsilon i} Z_{\beta i} \sqrt{\left| \frac{2000T_{Ni}}{b_i d_i^2} \frac{u_i + 1}{u_i} \right|}, \tag{5a}$$

$$\sigma_{FNi} = Y_{Fi} Y_{Si} Y_{\beta i} Y_{Bi} Y_{DTi} \left| \frac{2000T_{Ni}}{b_i d_i m_{ni}} \right|. \tag{5b}$$

In the above equations, Z_{Hi} , Z_{Ei} , $Z_{\epsilon i}$ and $Z_{\beta i}$ are the zone, elasticity, contact ratio and helix angle factors of i th gear which is selected based on each gear design according to ISO 6336-2 [17]. Y_{Fi} , Y_{Si} , $Y_{\beta i}$, Y_{Bi} and Y_{DTi} are the form, stress correction, helix angle, rim thickness and deep tooth factors calculated by following the procedure discussed in ISO 6336-3 [18] based on the gear geometry. b is the face width, d is the pitch diameter, m_n is the normal modulus and u is the gear ratio of the engaged gear pair ($u = \frac{z_2}{z_1} \geq 1$).

Bearings load calculation theory: The bearings in the power train are different types of radial roller and ball bearings designed to handle both radial and axial loads depending on their location. The assessment of the degradation of these bearings is performed based on the analysis of dynamic equivalent radial load for radial roller/ball bearings according to the procedure explained by ISO 281 stan-

dard [15] by using the equation $P_r = X F_r + Y F_a$, where F_r and F_a are the bearing’s radial and axial reaction forces. The life estimation based on this standard does not see the influence of wear, corrosion and electrical erosion on bearing life. The calculation of the dynamic loading factors X and Y for case of double-row roller bearings with nonzero contact angle γ which is the case for the under consideration bearings except the generator bearings and for the ball bearings used in the generator are according to ISO 281 [15].

The free body diagrams representing the applied and reaction loads on the three under consideration shafts, namely main shaft, gearbox (HSS) and generator shaft for load calculation for the corresponding bearings are shown in Fig. 4. The dynamic equivalent load calculation for the main bearings is performed based on the diagram in Fig. 4a. For the set of main bearings equations to be statically determinate, it is assumed that the 2nd main bearing MB-B is responsible for handing the axial forces. The latter is common practice in wind turbines, aimed at mitigating axial forces right before the gearbox. By writing the forces and moments equilibrium equations about the gearbox, the components of the bearings reaction forces will be

$$F_y^{MB-A} = M_z \left(\frac{1}{L_2 - L_1} \right) + B_y \left(\frac{L_2}{L_2 - L_1} \right), \tag{6a}$$

$$F_z^{MB-A} = M_y \left(\frac{1}{L_2 - L_1} \right) + B_z \left(\frac{L_2}{L_2 - L_1} \right) + G \left(-\frac{L_3 - L_2}{L_2 - L_1} \right), \tag{6b}$$

$$F_y^{MB-B} = M_z \left(-\frac{1}{L_2 - L_1} \right) + B_y \left(-\frac{L_1}{L_2 - L_1} \right), \tag{6c}$$

$$F_z^{MB-B} = M_y \left(-\frac{1}{L_2 - L_1} \right) + B_z \left(-\frac{L_1}{L_2 - L_1} \right) + G \left(\frac{L_3 - L_1}{L_2 - L_1} \right), \tag{6d}$$

$$F_x^{MB-B} = F_T, \tag{6e}$$

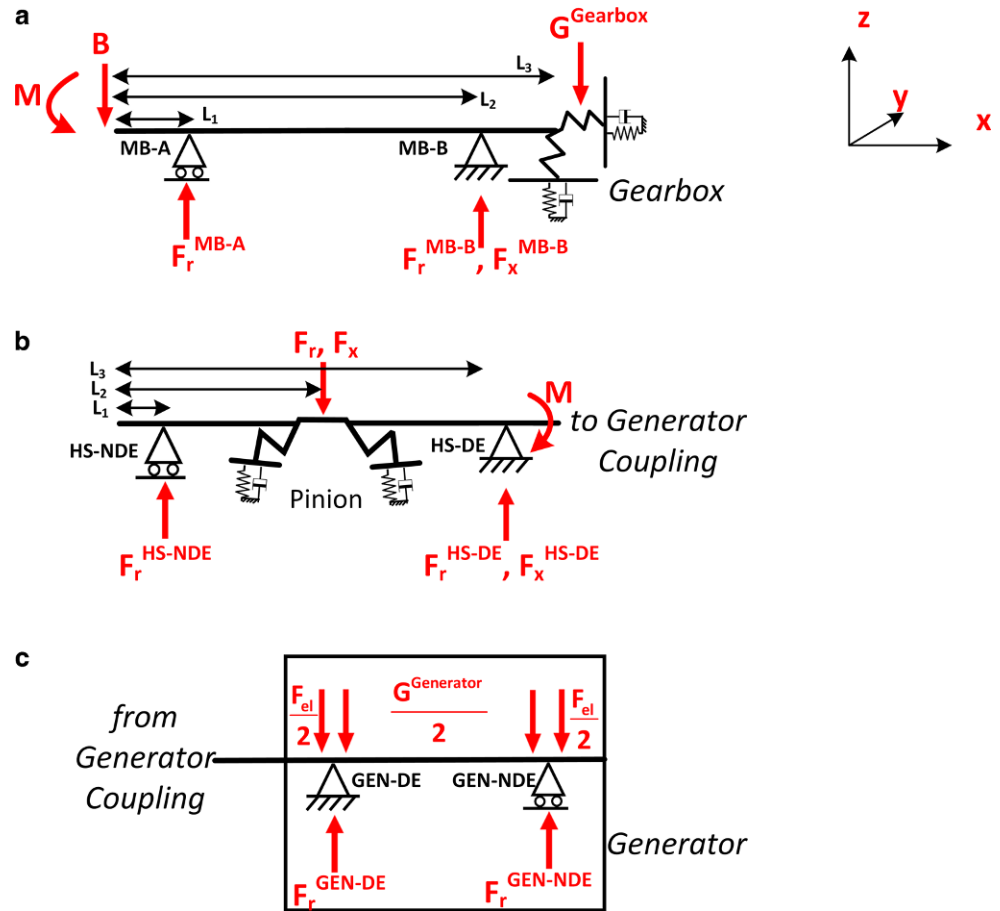
$$F_r^{MB-A} = \sqrt{(F_z^{MB-A})^2 + (F_y^{MB-A})^2}, \tag{6f}$$

$$F_r^{MB-B} = \sqrt{(F_z^{MB-B})^2 + (F_y^{MB-B})^2},$$

where M_y and M_z are nonrotating main shaft bending moments about the y- and z-axis, and B_y and B_z are nonrotating main shaft shear forces directed along the y- and z-axis, respectively. F_T is the main shaft thrust force. The equivalent radial dynamic loads of the two main bearings are then

$$P_r^{MB-B} = X F_r^{MB-B} + Y F_x^{MB-B}, \quad P_r^{MB-A} = F_r^{MB-A}. \tag{7}$$

Fig. 4 Free-body diagrams of the drivetrain shafts and bearings. **a** Main shaft and main bearings, **b** Gearbox HSS and bearings, **c** Generator shaft and bearings



Dynamic equivalent load calculation for the gearbox HSS bearings is based on the diagram shown in Fig. 4b. The equilibrium equations about HS-DE leads to the following simplified closed form equations

$$F_r^{HS-NDE} = \left| \frac{1}{L_3 - L_1} (F_r(L_3 - L_2) + M) \right|, \tag{8a}$$

$$F_r^{HS-DE} = |F_r - F_r^{HS-NDE}|, \quad F_x^{HS-DE} = |F_x|, \tag{8b}$$

where F_r^{HS-NDE} and F_r^{HS-DE} are the radial reaction forces on bearings HS-NDE and HS-DE. Bearing HS-DE is selected to handle the axial forces due to the helical pinion gear of the gearbox so that F_x^{HS-DE} is representing the axial reaction force of this bearing. M is the bending moment due to the weight of the part of the shaft located between bearing HS-DE and the generator coupling, which is assumed to be negligible. The forces on these two bearings due to the weight of gearbox HSS compared to the helical gear induced forces are also neglected. F_r and F_x are the radial and axial forces applied to the shaft by the helical gear as calculated by [4]

$$F_r = \frac{T_{pinion-s3} \tan \alpha_n}{d_{pinion} \cos \beta}, \quad F_x = \frac{T_{pinion-s3}}{d_{pinion}} \tan \beta, \tag{9}$$

where d_{pinion} is the pitch radius of pinion gear, α_n is the pressure angle in the normal direction, and β is the helix angle.

Dynamic equivalent load calculation for the generator bearings is based on the diagram shown in Fig. 4c. In this diagram, $G_{generator}$ is the force induced by the rotor weight on the bearings of the permanent magnet synchronous generator (PMSG). The rotor weight is modelled as the summation of weights of rotor yoke, generator shaft – including the part of the shaft which connects the generator to the flexible coupling – and the weight of surface-mounted permanent magnets. The F_{el} in this diagram represents the radial electromagnetic force in the air-gap surface area of the PMSG. The PMSG radial electromagnetic force is due to the interactions within or between armature reaction and permanent magnet fields including the stator slotting effect which is a function of tempo-spatial variations of $B_{\delta-r}$ as the radial component of air-gap magnetic flux density described by [7, 24]

$$B_{\delta-r} = \widehat{B}_\delta \sin \theta_{el}, \tag{10a}$$

$$F_{el} \approx \frac{B_{\delta-r}^2}{2\mu_0} = \frac{\widehat{B}_\delta^2}{2\mu_0} - \frac{\widehat{B}_\delta^2}{2\mu_0} \cos 2\theta_{el}. \tag{10b}$$

In the above equation, θ_{el} is the electrical angle which is a function generator speed $\theta_{el} = p\omega_{gen}$, where p is the number of pole pairs and ω_{gen} is the generator shaft speed. $B_{\delta-r}$ is approximated with the fundamental harmonic of the air-gap flux density, B_{δ}^1 , which is a function of the PMSG geometry. \hat{B}_{δ} is the peak value of the fundamental component of air-gap magnetic flux density measured for each pole. By using this approximation, the generator dynamic radial electromagnetic force is constructed of a constant and an oscillatory component which oscillate with double the generator electrical speed. The variations of air-gap thickness during operation and axial forces are neglected. The estimated electromagnetic force density is multiplied by rotor surface area to estimate the overall force. Both the static force due to the rotor of PMSG gravitational forces and the dynamic force due to radial electromagnetic force are assumed as concentrated forces which are applied equally to the two bearings. Therefore, the equivalent radial reaction forces on the two bearings $P_r^{GEN-NDE}$ and P_r^{GEN-DE} will be

$$F_z^{GEN-DE} = F_z^{GEN-NDE} = 0.5 (G^{Generator} + F_{el}), \tag{11a}$$

$$F_y^{GEN-DE} = F_y^{GEN-NDE} = 0.5 F_{el}, \tag{11b}$$

$$F_r^{GEN-DE} = F_r^{GEN-NDE} = 0.5 \sqrt{(G^{Generator} + F_{el})^2 + F_{el}^2}, \tag{11c}$$

$$P_r^{GEN-DE} = F_r^{GEN-DE}, P_r^{GEN-NDE} = F_r^{GEN-NDE}, \tag{11d}$$

where $F_r^{GEN-NDE}$ and F_r^{GEN-DE} are the radial reaction forces on bearings GEN-NDE and GEN-DE.

2.3.2 Power train system fatigue damage calculation

Gears degradation estimation: Fatigue damage estimation for the gears is performed by using the stress-life method. Each gear tooth surface pitting and root bending stresses are estimated as discussed in Sect. 2.3.1. The number of gear tooth contact stress cycles at different stress levels is counted by using time-domain rainflow cycle counting. The outputs are the amplitude stress level σ_s , and the number of stress cycles at σ_s for $s = (1, \dots, S)$. To consider the influence of nonzero mean stress level, Goodman rule is employed to calculate the effective stress (the equivalent zero mean alternating stress) by the equation, $\sigma_s^{eq} = \frac{\sigma_s}{1 - \frac{\sigma_s}{\sigma_u}}$, $\forall (s \in 1, \dots, S)$, where σ_m and σ_u are the mean stress and material yield strength, respectively. The damage for the data block t with S different stress levels σ_s^{eq} , ($s \in 1, \dots, S$) is calculated by using Palmgren-Miner rule as $D = \sum_{s=1}^S \frac{n_s}{N_s}$, where n_s is the number of cycles at the stress level σ_s^{eq} and N_s is the number of cycles to yield at stress level σ_s^{eq} , where $N_s = k(\sigma_s^{eq})^{(-m)}$. This procedure is carried out separately for both the gear pitting and root bending

stresses, and finally the maximum damage for i th gear is estimated by

$$D^{gear-i} = \max \left\{ D_{pitting}^{gear-i}, D_{root-bending}^{gear-i} \right\}. \tag{12}$$

The selection of S-N curve parameters for the gears is based on the allowable stress with respect to the gear material and production quality from ISO 6336-5 [19], and the exponent parameter and the number of load cycles of short and long life zones of S-N curve from ISO 6336-6 [20].

Bearings degradation estimation: The estimation of bearing damage is based on calculating the bearing dynamic equivalent load and using the bearing life equation according to the procedure explained in ISO 281 [15]. The wind turbine drivetrain bearings are all radial bearings with the basic rating life equation $L_{10} = (\frac{C_r}{P_r})^a$, where L_{10} is life with 90% reliability in million revolutions and C_r is the basic dynamic radial load rating in N obtained from the bearing manufacturer datasheet. The life exponent a is 3 for ball and 3.33 for roller bearings. Bearings' fatigue damage in this work is performed directly from the bearing equivalent dynamic load time series by using load-duration-distribution (LDD) approach [30]. The equations describing the functionality of LDD are

$$t = \sum_{i=1}^n t_i, l_i = t_i f_i, L_i = \left(\frac{C_r}{F_i} \right)^a, D = \sum_{i=1}^n \frac{l_i}{L_i}, \tag{13}$$

where D is the bearing damage during the time interval t , L_i is the time duration of the operation at load level F_i which causes the component to fail, and l_i is the time duration of the operation at the load level F_i . t_i is the time step length and f_i is the rotational frequency during t_i . The applied version of LDD goes through the load signal in time domain and accumulates the number of signal-revolutions at each load level by looking at the value of rotational speed at each time step. It also provides knowledge about how many revolutions result in bearing failure from the life equation. This method instinctively includes the effect of nonzero mean load, and in comparison with the the LDD based on load bins can give a more accurate value of damage.

2.3.3 Damage index definition

The above was about damage calculation for each component. In order to use damage in the farm controller, we need to consider a single damage indicator. However, we also want to identify the most important or vulnerable component and consider a damage index that can reflect this. Therefore a weighted average damage can be defined as damage indicator for each turbine. The damage indices explored in this research are explained in the following.

The index $DI^{overall}$ accounts equally for the damage of all the components as

$$DI^{overall}(u^{oc}, I^{oc}, DF^{oc}) = \frac{1}{M} \sum_{i=1}^M (D_i^{t,oc}(u^{oc}, I^{oc}, DF^{oc})), \tag{14}$$

where M is the number of components and $D_i^{t,oc}$ is the absolute value of accumulated damage for the component i , during the time interval t , and averaged on the different realizations of operating condition oc corresponded to average wind speed, turbulence intensity and derating factor $(u^{oc}, I^{oc}, DF^{oc})$. u , I and DF are the mean values during operation in time interval t . Another damage index can be defined by defining weight factors for each component based on average fatigue damage of component obtained from the probabilistic analysis of damage, which is defined as

$$DI_{weighted}^{overall}(u^{oc}, I^{oc}, DF^{oc}) = \frac{1}{M} \sum_{i=1}^M (\alpha_i D_i^{t,oc}(u^{oc}, I^{oc}, DF^{oc})), \quad s.t. \quad \sum_{i=1}^M \alpha_i = 1, \tag{15}$$

where α_i is a weight factor which represents the normalized damage for i th component obtained based on probabilistic long-term analysis of fatigue damage. The factor α_i identifies the importance or vulnerability of each component and uses it in the definition of the damage index. This factor is based on weighted averaging of damage for each drivetrain component for all the possible power production fatigue damage load cases as described by

$$\alpha_i = \frac{\bar{D}_i}{\max(\bar{D})}, \tag{16a}$$

$$\bar{D}_i = \frac{\int_{u^{cut-in}}^{u^{cut-out}} D_i(u, I, DF) \cdot f(u) du}{\int_{u^{cut-in}}^{u^{cut-out}} f(u) du} \quad \text{for } i = 1, \dots, M, \tag{16b}$$

where $f(u)$ is the Rayleigh distribution describing the mean wind speed distribution averaged in 10 min intervals, its parameters are chosen based on IEC class I turbines from IEC61400-1 standard [13]. The vulnerability map shown in Fig. 9 in Sect. 3 shows the results of long-term fatigue damage analysis by applying the theory explained above.

This damage index can also be defined in such a way to take into account the damage of only the two main bearings, the two bearings of the gearbox HSS, the gears of the gearbox or the two generator bearings by manually setting the weight factor α_i .

The weight factor α_i in the definition of damage index can also be defined in such a way to reflect the risk of loss of turbine due to a specific component failure. For this

purpose, the consequent downtime can also be added to the index definition.

$$DI_{weighted}^{overall}(u^{oc}, I^{oc}, DF^{oc}) = \frac{1}{M} \sum_{i=1}^M (\alpha_i \gamma_i D_i^{t,oc}(u^{oc}, I^{oc}, DF^{oc})), \quad s.t. \quad \sum_{i=1}^M (\alpha_i \gamma_i) = 1. \tag{17}$$

For example, for the four-point drivetrain suspension under consideration, an unequal downtime due to unequal installation efforts to replace/repair main bearings, gearbox and generator is expected. Assuming the consequent downtime of the main bearings is twice that of the gearbox and four times that of the generator, γ_i takes 2, 1 and 0.5 for main bearings, gearbox components and generator bearings, respectively.

2.4 Multi-objective active power control

Standard practice for power derating is currently uniform and passive, i.e. DF is constant over turbines and time (typically for one hour, following the update rate used in energy markets). APC is a suggested improvement consisting in dispatching derating factors over turbines in a dynamic manner. It might be used for power maximization, reference power tracking for grid support, or load mitigation [23]. In this study, it is assumed that the farm in curtailed operation so we focus on the second and third objectives, with priority set on the second: the power reference from the grid should be tracked at best, and remaining freedom may be used for fatigue damage mitigation. Fatigue damage based on the analysis of stress is set as the quantity of interest in this research and is believed to be more relevant than either load or damage equivalent load. It targets the actual value of components degradation and considers the nonlinearities between load and damage which is critical for estimating the degradation of gears.

In this work, focus is put on the effect of:

- Farm control on accumulated damage in the medium term (one to two weeks),
- Actively using current damage rate in the controller’s objectives,
- Power fluctuations arising from farm-wide turbulence, resulting in periods of low energy where power tracking is prioritised, and periods where freedom is left for fatigue damage mitigation.

2.4.1 Simulation setup

To calculate the mid-term accumulated fatigue damage, a setup using quasi-steady wake and turbine modelling

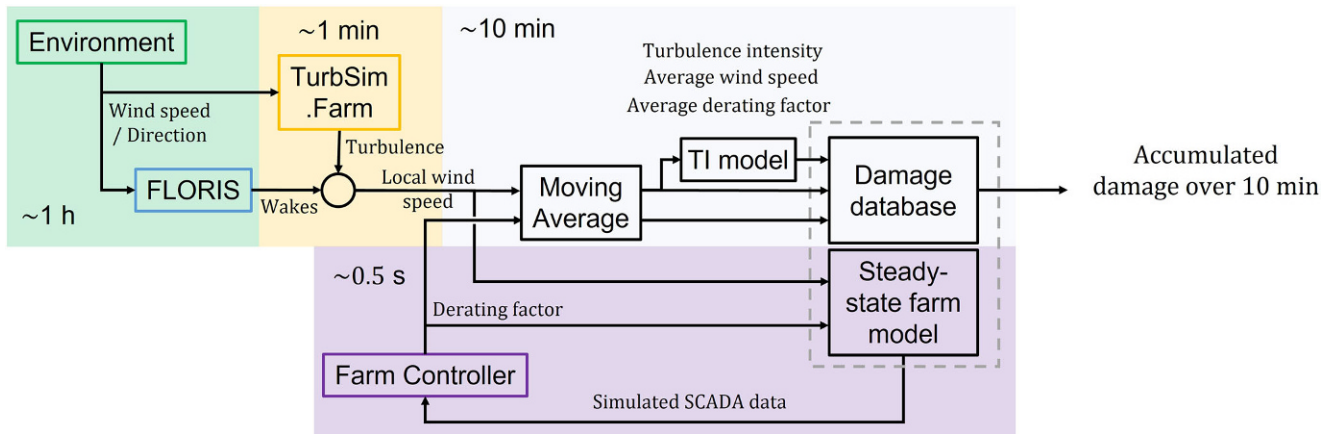


Fig. 5 Farm-level simulation setup

approach is devised, shown in Fig. 5. TurbSim.Farm is a farm-level synthetic turbulence generator described in [5]. NREL’s FLORIS is a steady-state farm flow model, here modified to encompass the effect of derating on wakes.

As introduced in Sect. 2.1, the wind speed u and derating factor DF are obtained from a 10-min moving average filter. DF is relative to available power, which is calculated using (1) and a rotor-averaged wind speed from a Kalman filter-based wind speed observer [10]. Turbulence intensity may also be observed from the turbine response, which should be the preferred way for real-world use of damage in wind farm control. In this work, turbulence intensity is computed from u through the simple added wake turbulence intensity model defined in the IEC 61400-1 standard [13]:

$$\begin{cases} I_{eff} = \frac{\sigma}{u} & d \geq 10 D \\ I_{eff} = \frac{[(1-2\pi p_w)\sigma^m + 2\pi p_w \sigma_T^m(d)]^{\frac{1}{m}}}{u} & d < 10 D \\ \sigma_T = \sqrt{\frac{0.9 u^2}{(1.5+0.3d\sqrt{u})^2} + \sigma^2} \end{cases}$$

where $p_w = 0.06$ is an empirical weight accounting for a possible upstream turbine at a distance d , and D the turbine diameter. σ is the standard deviation of ambient wind speed fluctuations matching the one used in the database’s

turbine-level simulation for the current mean wind speed (i.e. using the same turbulence class and standard version). m is the Wöhler curve exponent for the component under consideration. As the impact on turbulence intensity is relatively weak, a constant value (e.g. $m = -7$, typical for gears as seen in Table 2) may be used for simplicity.

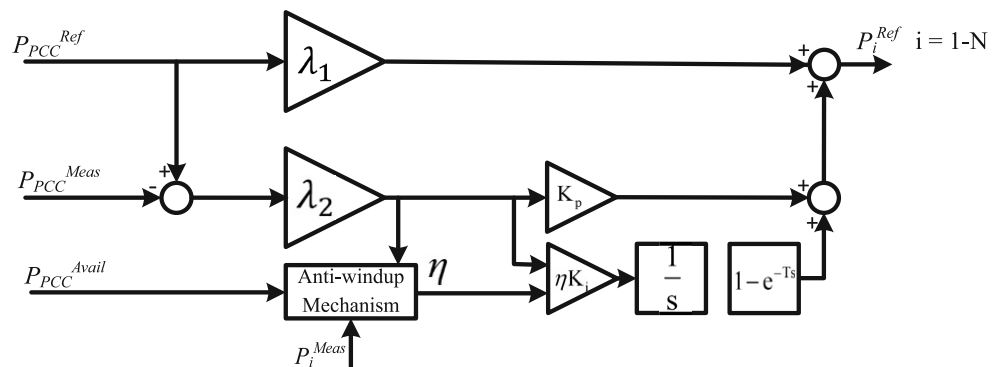
Using this efficient short-term simulation framework, the damage may be accumulated to medium term by summing on a distribution of 1-h environmental conditions of our choice.

2.4.2 Wind farm controller

The controller is an adapted version from [25]. This controller is based on a proportional-integral (PI) controller. This controller is hierarchical in the sense that it (1) does not alter turbine-level control and (2) prioritizes power tracking over fatigue damage mitigation. It may be put under the hood of distributed control, where each turbine is treated separately with limited knowledge about others (the only inputs transmitted from farm level are the reference and actual output powers and the total damage rate).

A block diagram is shown in Fig. 6. Adaptive gains $\lambda_j : j \in \{1, 2\}$ representing power dispatch are selected for each turbine according to the fatigue damage of power

Fig. 6 Farm APC



train system at each turbine as a function of wind condition and power demand. The feedforward terms theoretically provide the desired farm-level power at any time. The feedback term is to compensate for modelling uncertainties and actuation errors. λ_1 acts on feedforward and is hence more on mean power, while λ_2 acts on feedback and hence on power fluctuations. The mapping from damage to λ_j for turbine i is defined through the tunable function g_{ij} reading

$$\lambda_{ij} = \frac{g_{ij}(DI(u, I, DF))}{\sum_{turbines} g_{ij}(DI(u, I, DF))}, \quad s.t. \quad \sum_{i=1}^N \lambda_{ij} = 1. \tag{18}$$

3 Results and discussions

3.1 Creation of database and drivetrain degradation analysis

DLC 1.2 (power production based on normal turbulence model (NTM) over the wind speed range $V_{in} < V_{hub} < V_{out}$ is relevant in this study, which is concerned with fatigue loading during normal operation of a wind turbine throughout its lifetime. To be holistic in defining the wind input files for the proposed database, the average wind speed changes from 4 m/s to 25 m/s in steps of 2.1 m/s and turbulence intensity changes from 0 to 40% in steps of 4%. To account for wake influence in the turbulence intensity, added-wake turbulence intensity is considered. The derating factor DF changes from 0 to 100% in steps of 10%. All the conditions in IEC61400-1 [13] for valid wind turbine load calculations for fatigue damage analysis are met. IEC61400-1 and DNVGL-ST-0437 [6] require at least 6 independent realizations with the duration of at least 10 minutes for DLC 2.1. The simulations for the creation of database are carried out in 30 minutes intervals with 10 independent realizations for each operating condition. The first 10 minutes which may contain the transients are removed. Then the damage

indicators representing the damage at different operating conditions are calculated for all the operating conditions.

The $GenPwr$ shown in the results is the output power generated by the turbine which is the DF times the available power.

The power train system dynamic model in the global simulations – used for calculating the input loads for the power train components damage analysis – is a two degree of freedom (DOF) torsional model which is able to capture the interactions of the first mode with the rest of turbine and external excitations. The parameters including generator inertia, shaft flexibility and gear ratio are adopted from the medium-speed power train design proposed by [26]. The turbine controller parameters are tuned to ensure a stable operation over the range of input wind speed under consideration. The generator controller is operating in constant power mode. Power law exponent depends on atmospheric stability and changes with variations of mean wind speed and turbulence intensity. In this research, it takes the constant value 0.14 from IEC 61400-3 [14].

3.1.1 Turbine controller performance

The performance of the implemented derating controller is shown in Fig. 7 which shows how the pitch and rotor speed regulators collaborate – to deliver different amounts of demand – as shown by derating factor DF at different average wind speeds. β is the pitch angle.

3.1.2 Power train degradation analysis

The drivetrain configuration, bearings selection and geometrical parameters of the drivetrain and the generator of 10MW medium-speed power train used as input for the components load calculations are obtained from [26, 38], except for the generator bearings and coupling which are selected based on this work. The S-N curve parameters for the gears fatigue damage calculation are listed in Table 2.

Table 3 lists the values of C_r for the bearings of under consideration drivetrain.

Fig. 7 Derating controller performance

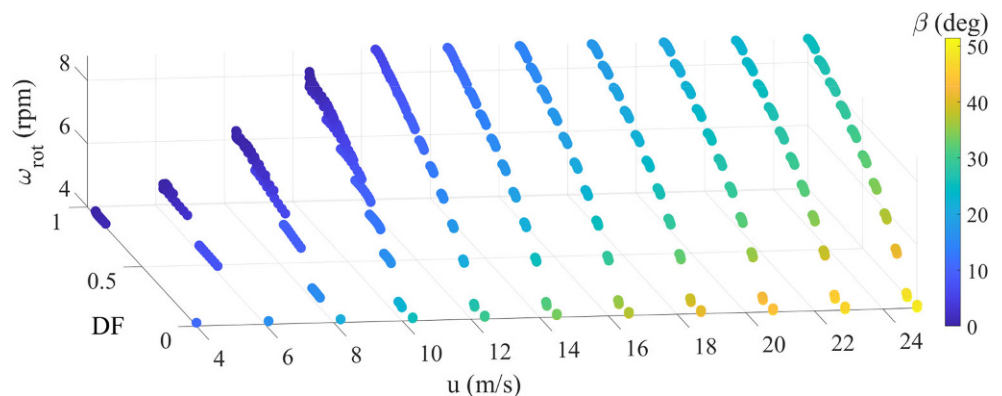


Table 2 S-N curve parameters for gear damage calculation

Fatigue mode	Gear	Material	Allowable stress	SN parameters
Pitting	Sun	18CrNiMo7-6 (Case hardened wrought steels)	1500	$6 \times 10^5 < N < 1 \times 10^7$: $m = 6.8, k = 33 \times 10^{27}$ $1 \times 10^7 < N < 1 \times 10^9$: $m = 8.8, k = 75 \times 10^{33}$ $1 \times 10^9 < N < 1 \times 10^{10}$: $m = 7.1, k = 77 \times 10^{28}$
	Planet			
Pitting	Ring	42CrMo4 (Through hardened wrought steels)	846	$6 \times 10^5 < N < 1 \times 10^7$: $m = 6.8, k = 28 \times 10^{25}$ $1 \times 10^7 < N < 1 \times 10^9$: $m = 8.8, k = 15 \times 10^{31}$ $1 \times 10^9 < N < 1 \times 10^{10}$: $m = 7.1, k = 52 \times 10^{26}$
Root bending	Sun	18CrNiMo7-6	425	$1 \times 10^3 < N < 3 \times 10^6$: $m = 8.7, k = 28 \times 10^{28}$ $3 \times 10^6 < N < 1 \times 10^{10}$: $m = 49.9, k = 47 \times 10^{136}$
	Planet			
Root bending	Ring	42CrMo4	340	$1 \times 10^4 < N < 3 \times 10^6$: $m = 6.2, k = 17 \times 10^{21}$ $3 \times 10^6 < N < 1 \times 10^{10}$: $m = 49.9, k = 67 \times 10^{131}$

Table 3 Basic dynamic load rating of the drivetrain bearings

Bearing	C_r (N)
MB-A	5.6431×10^6
MB-B	4.5774×10^6
HSS-NDE	2.16×10^6
HSS-DE	3.79×10^6
GEN-NDE	1.04×10^6
GEN-DE	1.04×10^6

The selected results of implementing the bearings equivalent dynamic load and the gears contact and bending stresses calculation explained in Sect. 2.3.2 are shown in Fig. 8. As it can be seen, to show the dependency of drivetrain components loads to the operating condition, in each figure, four different load cases with respect to different average wind speeds, turbulence intensities and derating factors are examined.

The vulnerability map of drivetrain components can be established based on long-term NTM fatigue damage analysis as shown in Fig. 9, which is the basis for defining weights in the weighted average damage index.

The Log-scale scattered view of damage index $DI_{overall}$ vs. mean wind speed, turbulence intensity and derating factor is shown in Fig. 10, which shows the influence of a wide range of variations in wind condition and power demand – presented by derating factor – on the overall fatigue damage of drivetrain system. This figure helps to see how the simultaneous variations of inputs influence the average damage. However, to see the influence of each input independently, a sensitivity analysis is performed with selected results reported in Fig. 11. As it can be seen in Fig. 11a which shows the drivetrain fatigue damage vs. mean wind speed varia-

tions, the damage is maximum around the rated wind speed, where a 10% reduction of demand, can reduce damage by 19%. Our observations show that the drivetrain component that contributes the most to the fatigue damage in this operating condition is the gearbox-side main bearing. As it can be seen in Fig. 11b showing the damage vs. turbulence intensity, the drivetrain maximum damage happens at maximum turbulence intensity, where 10% reduction of power demand can contribute to 13% reduction of damage. Our observations highlight planets of the 1st planetary gear stage as the damage critical component at operations in high turbulence intensities.

This study showed the different contribution of various drivetrain components in overall fatigue damage at different operating conditions. Our observations based on the drivetrain configuration under consideration showed that the damage of gears is sensitive the most to the variations of turbulence intensity, the damage of main bearings is sensitive the most to the variations of mean wind speed, and the damage of the gearbox HSS bearings and the generator bearings are sensitive the most to the variations of power demand.

This study also showed that fitting the polynomials of 6th order to damage versus actual power for different average wind speeds and turbulence intensities results in less than 1% relative average error for the wind speed range 4–25 m/s and the turbulence intensity range 0–32%. For instance, the 6th order polynomials fitting damage for the turbulence intensity $I = 12\%$ and average wind speed $u = 12.4$ m/s are shown in Fig. 11a and b, respectively. For the sake of simplicity, the coefficients of the polynomials are not shown in the figures.

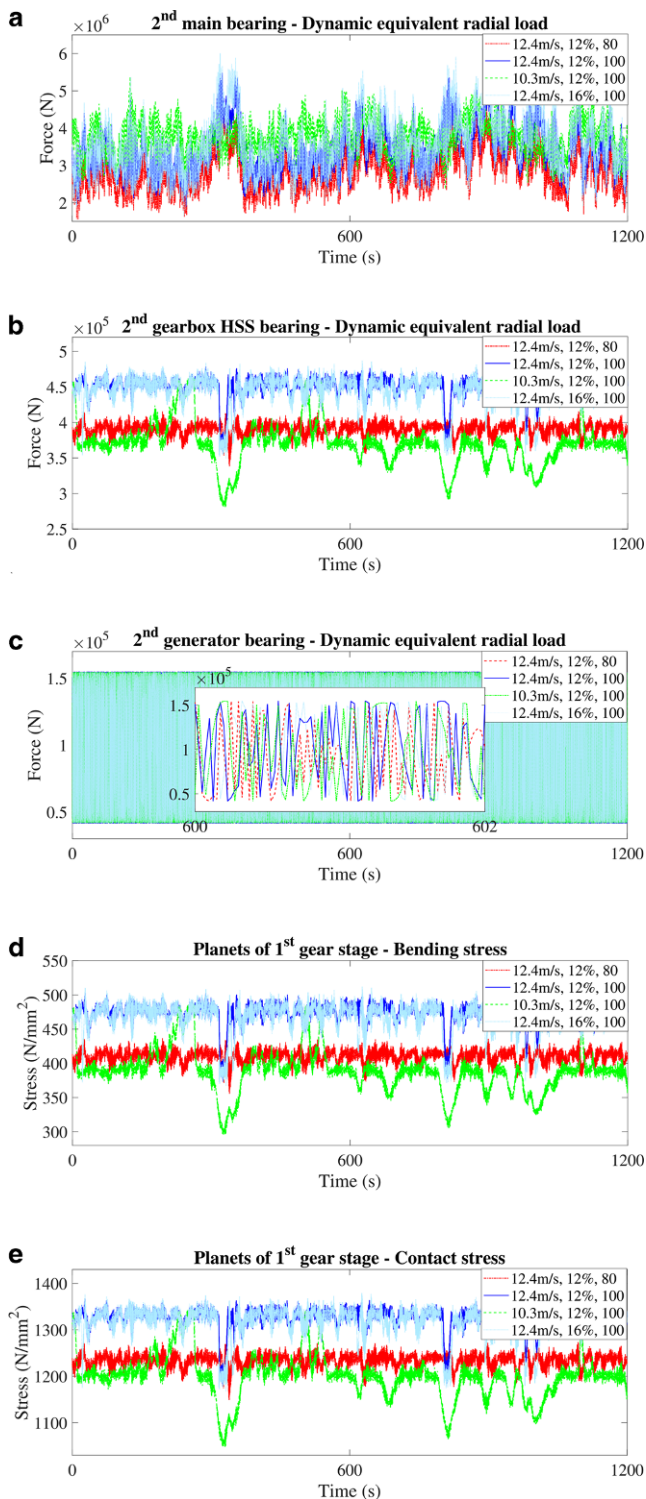


Fig. 8 Estimated drivetrain components load and stress by using the analytical models presented in Sect. 2.3.1 for different load conditions. **a** Main bearing MB-B equivalent radial dynamic load, **b** Gearbox bearing HSS-DE equivalent radial dynamic loads, **c** Generator bearing GEN-NDE equivalent radial dynamic load, **d** Bending stress on the planet gears of the 1st planetary gear stage (Planet-Stage1), **e** Contact stress on the planet gears of the 1st planetary gear stage (Planet-Stage1)

3.2 Demonstration of farm controller

A case study is performed on the TotalControl reference wind power plant (TC RWP) farm model consisting of 32 x DTU 10 MW turbines in a staggered 5D-spaced layout [1]. We look at the accumulated damage during one hour, with two different wind directions (West and North). Turbulence intensity is set as constant to 16% for simplicity (it showed not to have a significant impact in this particular case). The mapping function from damage to λ_i is tuned to

$$g_1 = g_2 = 1 - 0.5 \frac{DI_{overall} - DI_{min}^{overall}}{DI_{max}^{overall} - DI_{min}^{overall}},$$

i.e., the overall damage is used and normalized to [0,1], then mapped in a linear and uniform way between feedback and feedforward, while setting $\lambda_i = 0.5$ as lower bound. Other tuning parameters are irrelevant here.

When all turbines use the same database for damage index independent of their initial accumulated damage, the open-loop (without active power control) difference in damage comes down to whether or not the turbine is currently in wake flow. There, the effect of wake velocity deficit prevails on wake-induced turbulence, yielding higher damage on upstream than on downstream turbines. Depending on wind direction, upstream turbines are hence derated more while downstream turbines compensate to keep tracking the power reference. West wind is the dominant wind direction, with minimal wake effect (2 rows with 10D spacing), while North wind is unfavorable (8 rows with 5D spacing). The results are summarized in Fig. 12 where the accumulated damage for the wind farm turbines is illustrated for both cases. In Fig. 12a we notice the effect of considering damage in the farm control for the case of West wind. The load mitigation feature of controller tends to make the damage distribution over the turbines more uniform, shaving the peaks of accumulated damage as observed for turbines 3, 4, 8 and 32. From Fig. 12b we observe similar results but for the case of North wind. Now, the load mitigation effects are clearly observable for the northern most turbines (*i.e.*, turbines 1–12), those being affected the least by the wake effect in the farm.

When that is said, this case does not show the damage mitigation feature at its best. Indeed, the controller is rather designed for sparing one or a few already damaged turbine(s) than for reducing the mean damage over all turbines (although this can be improved by better tuning of the mapping functions g_i , $i \in \{1,2\}$). For a full demonstration of the proposed approach, a model for damaged turbine (for instance showing early signs of failure in the form of abnormal vibrations) would be valuable.

Fig. 9 Vulnerability map of drivetrain

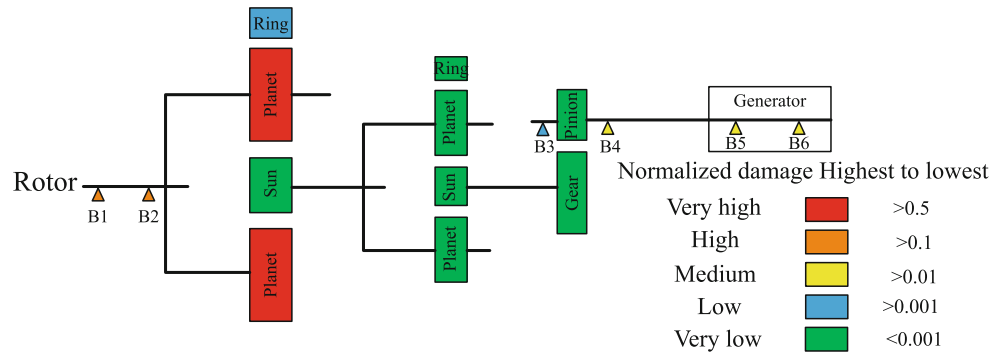
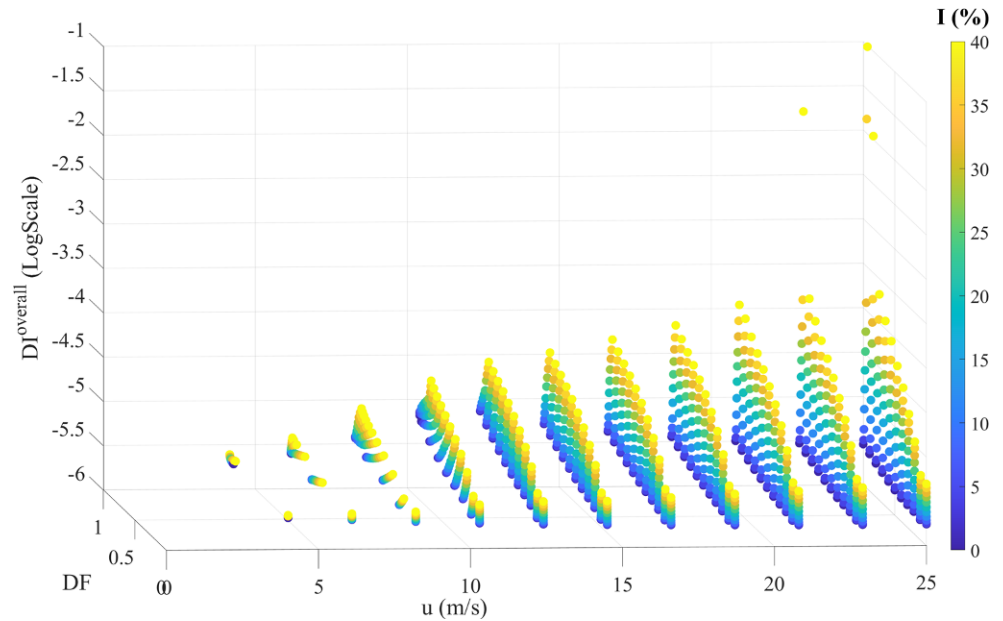


Fig. 10 Damage index vs. mean wind speed, turbulence intensity, derating factor



4 Conclusion

A database approach for accommodating the fatigue damage of wind turbine power train system in farm-level active power control is proposed and applied to the DTU 10 MW reference wind turbine. In this process, the relationship between the damage of the different drivetrain components and external conditions – namely wind conditions and power command from farm controller – is detailed and evaluated by means of aero-servoelastic simulations and degradation modelling based on IEC and ISO standards. The procedure includes the fatigue load and stress calculation at component level, the estimation of the components degradation and then the estimation of the weighted average damage of the drivetrain by doing a long-term damage analysis.

Results shows that reducing power demand has a clear positive influence on the drivetrain average damage, but variation as function of wind condition is significant. Use in multi-objective farm active power control has been demonstrated through a case study on the TotalControl reference

wind power plant. The demonstration results show success in evening out damage across turbines in the farm and hence the potential of the proposed fatigue damage mitigation approach in the damage peak shaving.

Further improvements include:

- Providing a database for faulty components to enable using the approach for mid-term maintenance planning and exploit the full potential of the farm controller’s fatigue damage-mitigation feature,
- Performing sensitivity analyses on known uncertainties and validate against higher-fidelity simulations at turbine and farm levels,
- Tuning the proposed farm controller to optimize the damage mitigation feature for various scenarios.

Acknowledgements This project has received funding from the Norwegian Research Council in the project CONWIND: Research on smart operation control technologies for offshore wind farms (grant no. 304229), and the Research Center NorthWind (grant no. 321954); and from the EU H2020 WATEREYE project (grant agreement no. 851207).

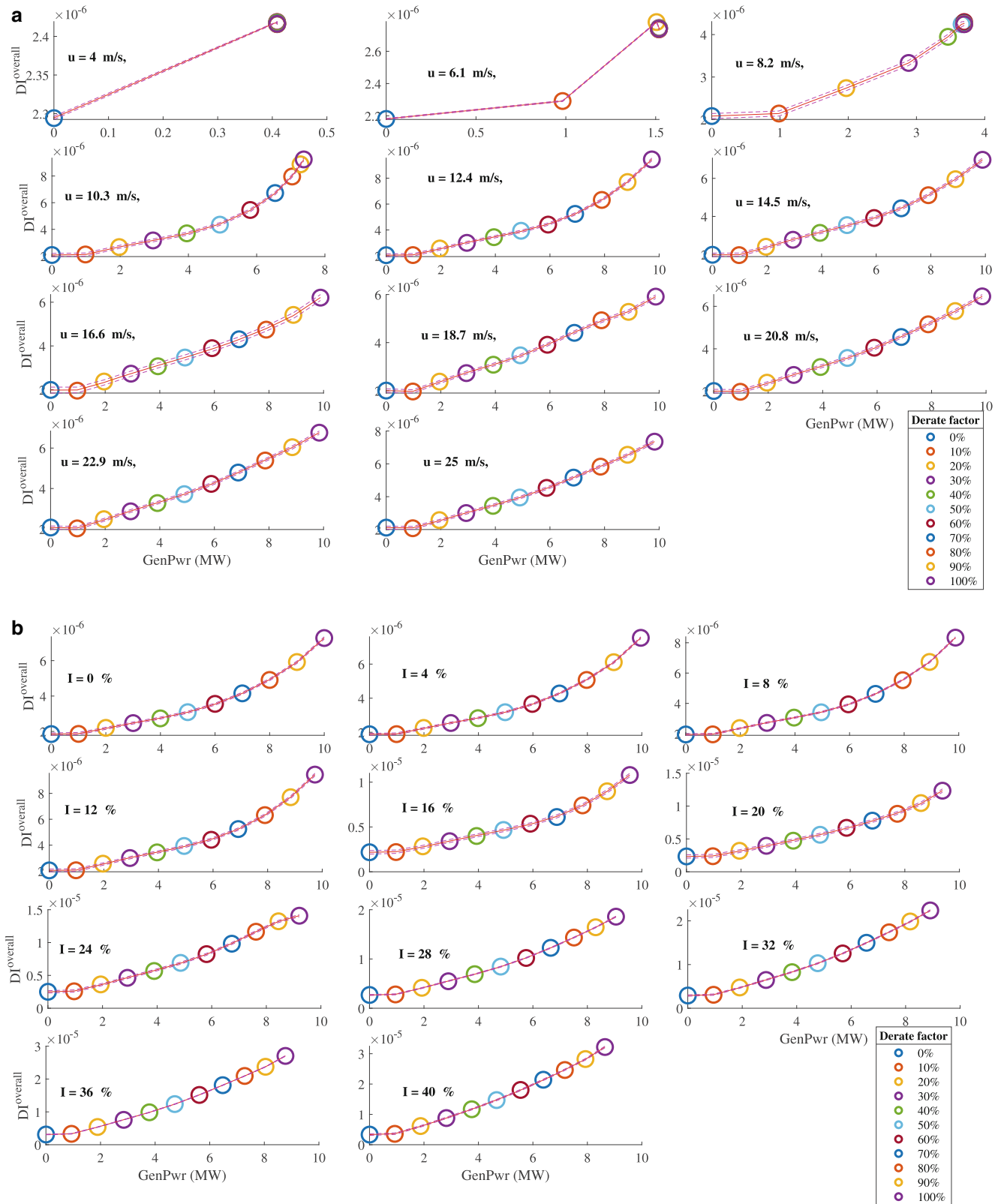


Fig. 11 Drivetrain fatigue damage vs. actual power sensitivity analysis. **a** Damage index vs. the power generated at turbulence intensity $I = 12\%$ and different wind speeds, **b** Damage index vs. the power generated at average wind speed $u = 12.4 \text{ m/s}$ and different turbulence intensities

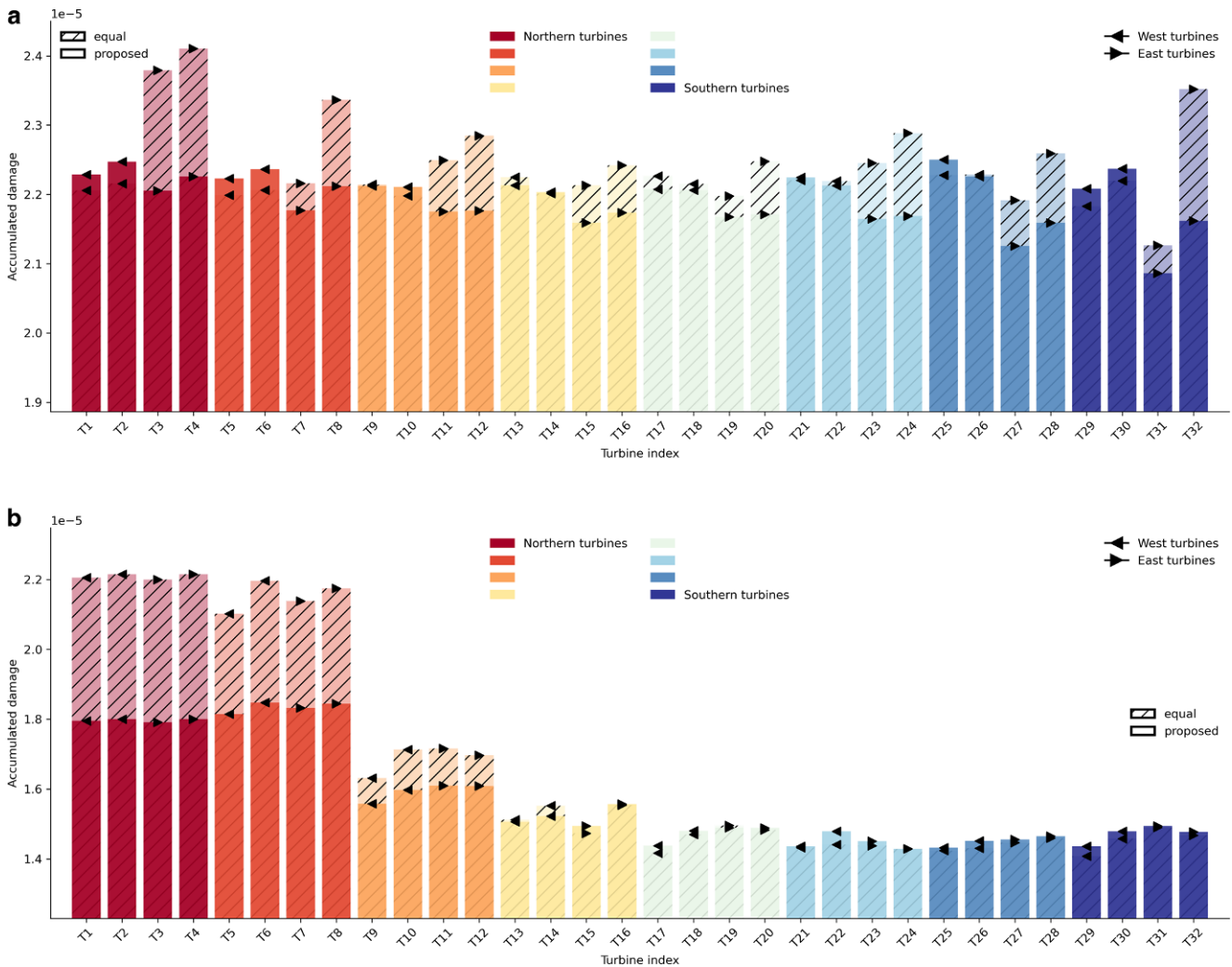


Fig. 12 Control strategies comparison regarding the accumulated damage for the farm turbines over one hour. **a** Wind coming from the West, **b** Wind coming from the North

Funding Open access funding provided by NTNU Norwegian University of Science and Technology (incl St. Olavs Hospital - Trondheim University Hospital)

Open Access This article is licensed under a Creative Commons Attribution 4.0 International License, which permits use, sharing, adaptation, distribution and reproduction in any medium or format, as long as you give appropriate credit to the original author(s) and the source, provide a link to the Creative Commons licence, and indicate if changes were made. The images or other third party material in this article are included in the article’s Creative Commons licence, unless indicated otherwise in a credit line to the material. If material is not included in the article’s Creative Commons licence and your intended use is not permitted by statutory regulation or exceeds the permitted use, you will need to obtain permission directly from the copyright holder. To view a copy of this licence, visit <http://creativecommons.org/licenses/by/4.0/>.

References

- Andersen SJ, Madariaga A, Merz K, Meyers J, Munters W, Rodriguez C (2018) Reference wind power plant d1.03
- Baros S, Annaswamy AM (2019) Distributed optimal wind farm control for fatigue load minimization: a consensus approach. *Int J Electr Power Energy Syst* 112:452–459
- van Binsbergen DW, Wang S, Nejad AR (2020) Effects of induction and wake steering control on power and drivetrain responses for 10 mw floating wind turbines in a wind farm. *J Phys Conf Ser* 1618:22044
- Budynas RG, Nisbett JK (2015) Shigley’s mechanical engineering design vol 10. McGraw-Hill, New York
- Chabaud V, Kölle K (2022) Real-time probabilistic analysis of wind farms. WATEREYE deliverable D4.2. SINTEF, Trondheim
- DNV-ST-0437:2021 (2021) DNV-st-0437:2021: Loads and site conditions for wind turbines. Standard, Det Norske Veritas AS, Oslo
- Eklund P, Eriksson S (2016) Air gap magnetic flux density variations due to manufacturing tolerances in a permanent magnet

- synchronous generator. In: 2016 XXII International Conference on Electrical Machines (ICEM). IEEE, pp 93–99
8. Fleming PA, Van Wingerden JW, Scholbrock AK, Van der Veen G, Wright AD (2013) Field testing a wind turbine drivetrain/tower damper using advanced design and validation techniques. In: 2013 American Control Conference. IEEE, pp 2227–2234
 9. Guo Y, Keller J (2020) Validation of combined analytical methods to predict slip in cylindrical roller bearings. *Tribol Int* 148:106–347
 10. Hansen MH, Henriksen LC (2013) Basic dtu wind energy controller
 11. Hart E, Turnbull A, Feuchtwang J, McMillan D, Golysheva E, Elliott R (2019) Wind turbine main-bearing loading and wind field characteristics. *Wind Energy* 22(11):1534–1547
 12. Hart E, Clarke B, Nicholas G, Kazemi AA, Stirling J, Carroll J, Dwyer-Joyce R, McDonald A, Long H (2020) A review of wind turbine main bearings: design, operation, modelling, damage mechanisms and fault detection. *Wind Energy Sci* 5(1):105–124
 13. IEC 61400-1:2019 (2019) IEC 61400-1:2019: Wind energy generation systems, part 1: Design requirements. Standard, International Electrotechnical Commission, Geneva, Switzerland
 14. IEC 61400-3-1:2019 (2019) IEC 61400-3-1:2019: Wind energy generation systems, part 3-1: Design requirements for fixed offshore wind turbines. Standard, International Electrotechnical Commission, Geneva, Switzerland
 15. ISO 281:2007 (2007) ISO 281:2007: Rolling bearings — dynamic load ratings and rating life. Standard, the International Organization for Standardization, Geneva, Switzerland
 16. ISO 6336-1:2019 (2019) ISO 6336-1:2019: Calculation of load capacity of spur and helical gears — part 1: Basic principles, introduction and general influence factors. Standard, the International Organization for Standardization, Geneva, Switzerland
 17. ISO 6336-2:2019 (2019) ISO 6336-2:2019: Calculation of load capacity of spur and helical gears — part 2: Calculation of surface durability (pitting). Standard, the International Organization for Standardization, Geneva, Switzerland
 18. ISO 6336-3:2019 (2019) ISO 6336-3:2019: Calculation of load capacity of spur and helical gears — part 3: Calculation of tooth bending strength. Standard, the International Organization for Standardization, Geneva, Switzerland
 19. ISO 6336-5:2016 (2016) ISO 6336-5:2016: Calculation of load capacity of spur and helical gears — part 5: Strength and quality of materials. Standard, the International Organization for Standardization, Geneva, Switzerland
 20. ISO 6336-6:2019 (2019) ISO 6336-6:2019: Calculation of load capacity of spur and helical gears — part 6: Calculation of service life under variable load. Standard, the International Organization for Standardization, Geneva, Switzerland
 21. de Jesus Barradas-Berglind J, Wisniewski R, Soltani M (2015) Fatigue damage estimation and data-based control for wind turbines. *IET Control Theory Appl* 9(7):1042–1050
 22. Kirsch J, Kyling H (2021) Optimized cast components in the drive train of wind turbines and inner ring creep in the main bearing seat. *Forsch Ingenieurwes* 85(2):199–210
 23. Knudsen T, Bak T, Svenstrup M (2015) Survey of wind farm control—power and fatigue optimization. *Wind Energy* 18(8):1333–1351
 24. Lin Y, Sun Y, Wang Y, Cai S, Shen JX (2021) Radial electromagnetic force and vibration in synchronous reluctance motors with asymmetric rotor structures. *IET Electr Power Appl* 15(9):1125–1137
 25. Merz K, Chabaud V, Garcia-Rosa PB, Kolle K (2021) A hierarchical supervisory wind power plant controller. *J Phys Conf Ser* 2018:12026. <https://doi.org/10.1088/1742-6596/2018/1/012026>
 26. Moghadam FK, Nejad AR (2020) Evaluation of pmsg-based drivetrain technologies for 10-mw floating offshore wind turbines: Pros and cons in a life cycle perspective. *Wind Energy* 23(7):1542–1563
 27. Moghadam FK, Vrana TK (2022) Wind power plant grid-forming control and influences on the power train and power system oscillations. In: The 11th Renewable Power Generation Conference – RPG 2022 IET, pp 2227–2234
 28. Moghadam FK, Rebouças GFS, Nejad AR (2021) Digital twin modeling for predictive maintenance of gearboxes in floating offshore wind turbine drivetrains. *Forsch Ingenieurwes* 85(2):273–286
 29. Natarajan A (2022) Damage equivalent load synthesis and stochastic extrapolation for fatigue life validation. *Wind Energy Sci* 7(3):1171–1181
 30. Niederstucke B, Anders A, Dalhoff P, Grzybowski R (2003) Load data analysis for wind turbine gearboxes
 31. Openfast documentation. <https://ap-openfast.readthedocs.io/en/mdv2-farm/source/user/index.html>. Accessed 9 Sept 2022
 32. Pagitsch M, Jacobs G, Bosse D (2020) Remaining useful life determination for wind turbines. *J Phys Conf Ser* 1452:12052
 33. Pagitsch M, Jacobs G, Bosse D, Duda T (2020) Estimation of internal gearbox loads for condition monitoring in wind turbines based on physical modeling. *J Phys Conf Ser* 1669:12008
 34. Pfaffel S, Faulstich S, Rohrig K (2017) Performance and reliability of wind turbines: a review. *Energies* 10(11):1904
 35. Silva JG, Doekemeijer BM, Ferrari R, van Wingerden JW (2022) Active power control of wind farms: an instantaneous approach on waked conditions. *J Phys Conf Ser* 2265:22056
 36. UpWind N (2011) Design limits and solutions for very large wind turbines. EWEA, Brussels
 37. Vali M, Petrović V, Steinfeld G, Pao YL, Kühn M (2019) An active power control approach for wake-induced load alleviation in a fully developed wind farm boundary layer. *Wind Energy Sci* 4(1):139–161
 38. Wang S, Nejad AR, Moan T (2020) On design, modelling, and analysis of a 10-mw medium-speed drivetrain for offshore wind turbines. *Wind Energy* 23(4):1099–1117
 39. Whittle M, Trevelyan J, Shin W, Tavner P (2014) Improving wind turbine drivetrain bearing reliability through pre-misalignment. *Wind Energy* 17(8):1217–1230
 40. Zhang P, Du Y, Habetler TG, Lu B (2010) A survey of condition monitoring and protection methods for medium-voltage induction motors. *IEEE Trans on Ind Applicat* 47(1):34–46